INSTITUTE OF PHYSICS PUBLISHING JOURNAL OF MICROMECHANICS AND MICROENGINEERING

J. Micromech. Microeng. **16** (2006) 1825–1832 doi:10.1088/0960-1317/16/9/010

Characterization of micromanipulator-controlled dry spinning of micro- and sub-microscale polymer fibers

Scott M Berry[1,2], **Steven A Harfenist**[2,4], **Robert W Cohn**[2] **and Robert S Keynton**[1,2,3]

[1] Department of Mechanical Engineering, University of Louisville, Louisville, KY 40292, USA
[2] ElectroOptics Research Institute and Nanotechnology Center, University of Louisville, Louisville, KY 40292, USA
[3] Department of Bioengineering, University of Louisville, 437 Lutz Hall, Louisville, KY 40292, USA

Received 17 March 2006, in final form 30 June 2006
Published 28 July 2006
Online at stacks.iop.org/JMM/16/1825

Abstract

No current microfabrication technique exists for producing room-temperature, high-precision, point-to-point polymer micro- and sub-microscale fibers in three dimensions. The purpose of this work is to characterize a novel method for fabricating interconnected three-dimensional (3-D) structures of micron and sub-micron feature size. Poly-(methyl methacrylate) (PMMA) micro- and sub-microscale fiber suspended bridges are fabricated at room temperature by drawing from pools of solvated polymer using a nano-tipped stylus that is precisely positioned by an ultra-high-precision micromilling machine. The fibers were drawn over a 1.8 mm silicon trench, and as the solvent in the solution bridge rapidly evaporates, a suspended, 3-D PMMA fiber remained between the two pools. The resulting fiber diameters were measured for solutions of PMMA in chlorobenzene with concentrations ranging from 15.5 to 23.0 wt% 495k g mol^{-1} PMMA and 13.0 to 21.0 wt% 950k g mol^{-1} PMMA. Fibers were found to increase in diameter from 450 nm to 50 μm, roughly corresponding to the increase in concentration of PMMA. To minimize fiber diameter variance, different stylus materials were investigated, with a Parylene®-coated stylus producing fibers with the lowest variance in diameter. Overall, the fiber diameter was found to increase significantly as the solution concentration and polymer molecular weight increased.

(Some figures in this article are in colour only in the electronic version)

1. Introduction

If micro- and sub-microscale fibers could be precisely placed, they could be integrated into microelectromechanical systems (MEMS) platforms providing complex three-dimensional assemblies of fibers. These suspended fibers could offer unique ways to couple between mechanical and guided-optical components [1, 2] as well as three-dimensional electrical connections for polymers impregnated with electrically conductive materials. Polymer fibers are routinely fabricated by a number of industrially-proven processes including wet, dry and melt spinning [3–20]. Dry spinning involves the extrusion of a polymer solution through orifices that shape

[4] Current address: Department of Physics, California Polytechnic State University, San Luis Obispo, CA 93407, USA.

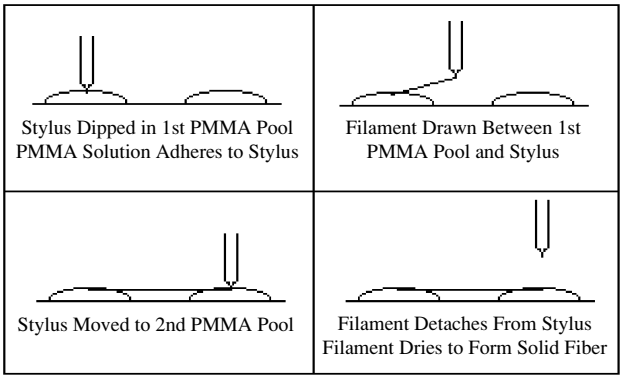

Figure 1. Schematic of the method of drawing micro- and nanofibers between two solvated PMMA pools.

the polymer solution into several fibers [3]. Wet spinning is nearly identical to dry spinning, except a secondary fluid is used to draw the solvent from the solution after extrusion and has been used to draw fibers with diameters ranging from 100 μm to over a millimeter [4–8]. Melt spinning is another related process involving the extrusion of a melted polymer through an orifice, which yields fiber diameters ranging from tens of microns to millimeters [9–14]. Only electrospinning, which involves utilizing a strong electric field to shape a solvated polymer pendant drop into a fiber, produces sub-micron diameter fibers [15–19]. The fiber is generally collected as a randomly woven mat, though recently, mats with directionally-oriented weaves have been reported [20]. All of these processes serve some industrial niche, but none of them allows for the precise, controlled placement of individual micron-/sub-micron-sized fibers on a substrate.

Recently, a technique has been reported that can be used to custom pattern suspended, polymer nanofibers in three dimensions [1, 21]. It involves dipping a stylus into a pool of solvated polymer, allowing the solution to adhere to the stylus tip, and removing the stylus from the pool, leaving a solution filament extending between the pool and stylus (figure 1). If the stylus is dipped into a second solution pool, the filament will detach from the stylus and remain suspended between the two pools. Upon complete evaporation of the solvent, a solid, rounded polymer fiber is produced, suspended between the two pools. Suspended geometries, such as these, require several, more involved processing steps when fabricated with traditional planar microfabrication techniques. A needed improvement to the method presented in [1, 21] is the ability to select the processing conditions that yield a fiber with a desired diameter. Therefore, the goal of this work is to characterize the process introduced in [1] by developing empirical relationships between experimental parameters and fiber diameter.

2. Methodology

2.1. Solution preparation and characterization

In this study, several parameters are varied, including polymer concentration in the solution, polymer molecular weight and the material coating of the stylus. The dependence of diameter on individual parameters was investigated, including a comparison with the dimensionless, 'processability parameter',

$$P = \frac{k\eta}{\sigma}, \tag{1}$$

which combines the influence of viscosity η, solvent evaporation rate k and surface tension σ [22]. According to the theory of Tripathi *et al* [22], for the same fiber drawing conditions (e.g. length and drawing speed), the same fiber diameter will form as long as the three individual parameters produce the identical value of P.

Several different concentrations of poly-methyl methacrylate (PMMA) in chlorobenzene were made from stock solutions of MicroChem C9 Series Photoresist (495k g mol^{-1} and 950k g mol^{-1} average polymer molecular weight, MicroChem Inc., Newton, MA) by diluting with chlorobenzene and thickening by evaporation of the chlorobenzene. Initial experiments illustrated that fibers could be successfully drawn from polymer solutions ranging in concentration from 15.5 to 23.0 wt% for the 495k g mol^{-1} PMMA and 13.0 to 21.3 wt% for the 950k g mol^{-1} PMMA. For solutions more dilute than these concentrations, the fibers would break up due to excessive capillary thinning prior to solidification; whereas, for overly concentrated solutions, the high viscosity led to ungainly, non-uniform structures. For each of the concentrations studied the individual parameters in equation (1) were measured (as described below) from which the processability parameter was calculated.

2.1.1. Viscosity. An LVDV-II+ viscometer (Brookfield, Middleboro, MA) interfaced with a cone-and-plate (CP-40 and CP-41, Brookfield) was used to measure the viscosities of PMMA/chlorobenzene solutions. The concentrations measured included 1%, 2.5%, 3.5%, 5%, 7%, 9%, 11.7%, 17.6% and 23.4% for the 495k g mol^{-1} PMMA and 1%, 2.5%, 3.5%, 5%, 7%, 9%, 11.2%, 14.9%, 18.6% for the 950k g mol^{-1} PMMA. A water jacket (TC-500 Refrigerated Bath/Circulator, Brookfield, Middleboro, MA) was employed to maintain the solutions at 22.0 °C. For both molecular weights, the viscosity correlates well exponentially with the solid weight fraction (SWF) with $\eta = 7.0256e^{46.828SWF}$ and $R^2 = 0.9704$ for 495k MW PMMA and $\eta = 3.476e^{34.721SWF}$ and $R^2 = 0.9847$ for the 950k MW PMMA (figure 2). This exponential relationship departs from the linear Einstein viscosity relationship, which suggests a significant interaction between adjacent polymer molecules in solution [23].

2.1.2. Surface tension. The surface tensions of the solutions were measured using the capillary method. A capillary was submerged into a beaker of the solution and the solution was allowed to rise into the capillary until equilibrium was reached. The height the fluid climbed above the fluid level in the beaker was measured and a close-up photograph was taken to determine the contact angle between the fluid and the capillary wall. The surface tension was given by [24]

$$\sigma = \frac{\rho \cdot r \cdot h \cdot g}{2\cos\theta}, \tag{2}$$

where ρ is the density of the solution, r is the radius of the capillary, h is the height of the climb, g is the gravitational acceleration and θ is the contact angle between the solution and the capillary wall. The density was measured to be

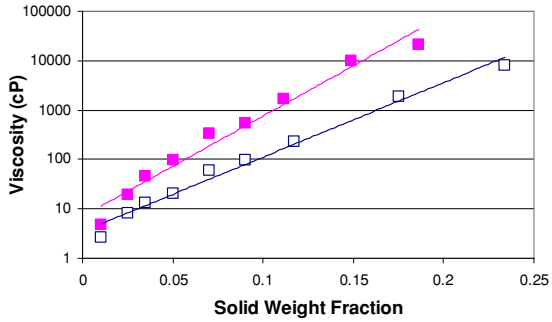

Figure 2. Viscosity of PMMA solution as a function of concentration. The upper and lower measured data and regression curves ($\eta = 3.476\ e^{34.721SWF}$ with $R^2 = 0.9847$ and $\eta = 7.0256\ e^{46.828SWF}$ with $R^2 = 0.9704$) are for the 950 k MW and 495k MW PMMA solutions, respectively.

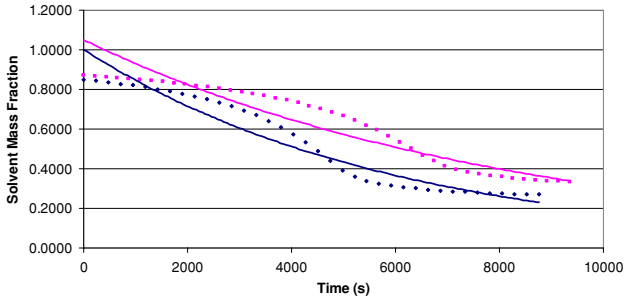

Figure 3. Solvent mass fraction for PMMA-chlorobenzene solutions as a function of time and molecular weight. The lower dotted and upper dotted lines represent the actual data recorded by the TGA for the 495k g mol^{-1} polymer and 950k g mol^{-1} polymer, respectively. Exponential regression analysis, indicated by the lower and upper solid lines, respectively, was performed on the TGA data in order to calculate the processability parameter.

1160k g m^{-3} for the 495k g mol^{-1} MW and 1240k g m^{-3} for the 950k g mol^{-1} MW. Compared to the viscosity, the surface tension was found to be relatively independent of concentration and equal to 0.039 N m^{-1} and 0.041 N m^{-1} for the 495k g mol^{-1} and 950k g mol^{-1} solutions, respectively.

2.1.3. Solvent evaporation rate. To quantify and normalize the solvent evaporation rate, a thermogravimetric analysis (TGA) was performed using a TA Instruments TGA 2950 (New Castle, DE) in order to extract a time constant governing this parameter. A 9% solution of each molecular weight PMMA was exposed to air for several hours, allowing the volatile chlorobenzene to evaporate, during which, the TGA recorded the mass of the solution at 5 s intervals. The solvent concentrations of both solutions were calculated and plotted over the drying time (figure 3). As performed in [22], solvent evaporation rate time constants were calculated by extracting the exponential coefficients from the exponential regression curves to each data set in figure 3. Although exponential curves do not capture the points of inflection seen in the data in figure 3, their high R^2 values suggest that they do accurately model the general rate of solvent evaporation while providing the needed coefficient. The lower curve ($SMF = 1.000e^{-(1.68\times10-4)t}$, $R^2 = 0.94$) represents the 495k g mol^{-1} data and the upper curve ($SMF = 1.050e^{-(1.68\times10-4)t}$, $R^2 = 0.92$) represents the 950k g mol^{-1} data, where SMF is the solvent mass fraction of the solutions. These coefficients were then normalized by dividing them by the surface area-to-volume ratio of the TGA samples (785 m^{-1}) to produce final time constant values of $2.14e^{-7}$ m s^{-1} and $1.54e^{-7}$ m s^{-1} for the 495k g mol^{-1} and 950k g mol^{-1} solutions, respectively.

2.2. Fiber diameter characterization

Each characterization trial consisted of drawing several fibers in rapid succession (approximately one fiber for every 8 s) back and forth between two 50 μL pools of solution. The pools were manually deposited by micropipette. The stylus is a sharpened tungsten wire with a 20 nm tip radius. The stylus was automatically positioned by a programmable, custom-made ultra-high-precision micromilling machine (Dover Instruments, Inc.) capable of translating in 1.25 nm increments in the horizontal X and Y directions and in 20 nm increments in the Z direction (figure 5) [25]. The stylus was dipped 50 μm into a solvated PMMA pool and moved in a serpentine motion between the two pools at a velocity of 5 mm s^{-1} (figure 4) in the same manner as described in figure 1. In order to produce suspended fibers, the solution pools were positioned on opposing sides of a 1.8 mm wide by 400 μm deep trench cut into a silicon substrate using a dicing saw (DAD 321, Disco, Tokyo, Japan). One trial was run for each of six different concentrations (15.5%, 16%, 17%, 18%, 21.6% and 23%) for the 495k g mol^{-1} polymer and each of four different concentrations (13%, 15%, 18% and 21.3%) for the 950k g mol^{-1} polymer. The diameters of the fibers were measured using a scanning electron microscope (SEM) (Carl Zeiss LEO Supra 35) with a variable pressure secondary electron detector (VPSE) that operates in a non-conductive mode, allowing the nonconductive polymer fibers to be imaged without a metal overcoat. The diameter of each fiber that spanned the trench without breaking or sagging was measured in three locations (in the middle and near each end) and averaged.

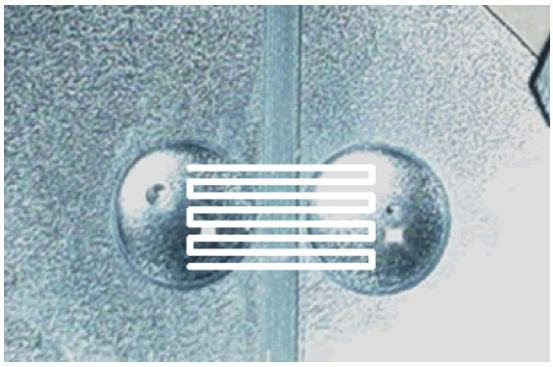

Figure 4. Solution deposited on silicon substrate immediately before trial run. The line indicates the serpentine path taken by the stylus.

3. Results and discussion

3.1. Fiber diameter measurements

Fibers with diameters ranging from 450 nm to 50 μm were drawn spanning the 1.8 mm trench without breaking or

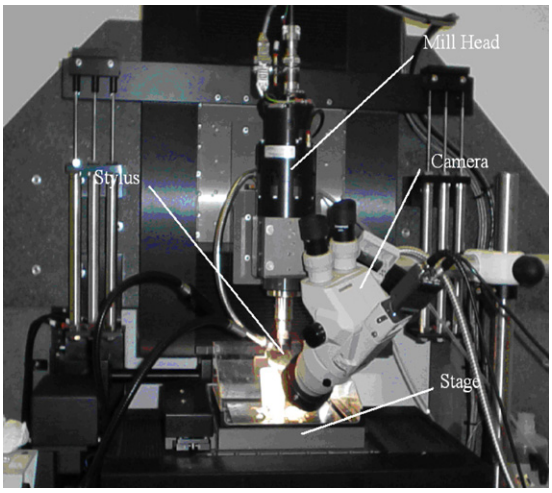

Figure 5. Dover instruments micromilling machine—the stage which contains the substrate material translates in the horizontal plane whereas the stylus, which is attached to the mill head, translates vertically.

sagging (figure 6). These suspended fibers were cylindrically symmetric with only a slight tapering occurring at each end (figure 6(*d*)) and were observed to be rigid, with no gravitationally-induced bending. The resulting fiber diameters are reported as a function of concentration (figure 7). For this processing technique, the standard deviation of the diameter was as large as 11.0 μm. One possible cause for this variance was the uncontrolled build-up of solution and dried PMMA on the stylus tip that accumulated over the course of each trial (figure 8). Surface treatments to the stylus were considered next as a way to affect wetting and/or surface tension of the polymer-stylus interface to reduce the effect of excess accumulation. Fibers were drawn with styli coated with Parylene® (poly-para-xylylene), and perfluorooctyl-trichlorosilane (a nonstick material used for separating hot embossed PMMA from its master stamp), as well as with a tapered glass capillary (tip radius of 10 μm). The Parylene®-coated stylus provided a substantial improvement in diameter variation over the original tungsten stylus, yielding the best overall reduction in diameter variance for all coatings, with an average standard deviation of 2.06 μm and a maximum standard deviation of 3.02 μm for the six tested concentrations of the 495k g mol^{-1} polymer (table 1).

3.2. Direct-write, continuous drawing of PMMA fibers

In an effort to broaden the applicability of this process, a direct-write method of fabrication was developed. This method replaced the stylus with a 1 mm (inner diameter) glass capillary filled with PMMA solution and affixed to the micromilling machine. A clamp attached to the capillary bulb was tightened in order to pressurize the capillary, thereby expelling PMMA solution from the capillary tip. This clamp was adjusted to apply a pressure sufficient to expel the various solutions at flow rates of approximately 20 μL min^{-1}. The capillary tip was positioned 500 μm above an untreated silicon wafer substrate and the expelled solution was allowed to contact the substrate. Once contact had been established, the micromill was programmed to lift the capillary 2 mm in the vertical direction and translate its distances ranging from 2 mm to 50 mm in the horizontal plane, forming a filament of PMMA solution anchored to the substrate at the point of initial contact. Additional anchor points were then generated by lowering the

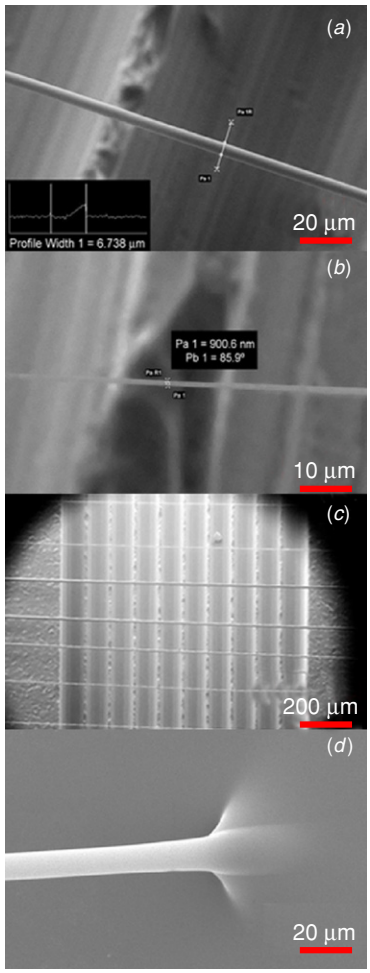

Figure 6. SEM images of polymer fibers drawn over a 1.8 mm trench. (*a*) Suspended fiber drawn from 15% solution of 950k g mol^{-1} PMMA. (*b*) Suspended fiber drawn from 13% solution of 950k g mol^{-1} PMMA. (*c*) Several parallel fibers drawn from 15.5% solution of 495k g mol^{-1} PMMA. (*d*) Tapered end of PMMA fiber.

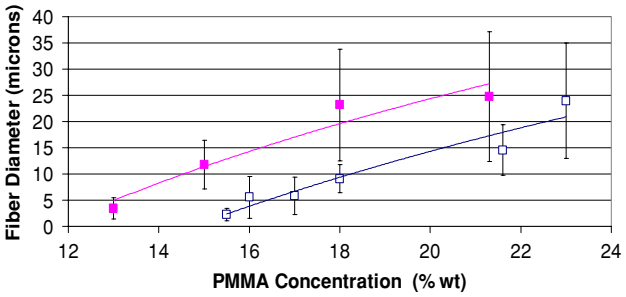

Figure 7. Fiber diameter versus concentration. The hollow and solid data points represent the average measured diameters of the drawn fibers for the 495k g mol^{-1} data and the 950 g mol^{-1} data, respectively. The error bars represent the standard deviation of each data point.

Table 1. Fiber diameters: mean and standard deviation (in microns) for fibers drawn with 495k g mol^{-1} PMMA solutions using different stylus material coatings.

Concentration (wt%)	Tungsten (μm)	Glass (μm)	Parylene (μm)	Nonstick (μm)
15.5	2.22 ± 1.20	2.43 ± 1.09	No data	10.81 ± 6.88
16	5.54 ± 3.95	4.38 ± 3.11	7.41 ± 2.49	8.76 ± 2.84
17	5.80 ± 3.59	4.20 ± 2.04	6.78 ± 1.38	7.92 ± 5.08
18	9.07 ± 2.68	4.84 ± 2.71	6.27 ± 3.02	4.69 ± 2.69
21.6	14.53 ± 4.82	18.37 ± 6.36	19.03 ± 1.40	15.24 ± 7.58
23	23.96 ± 11.00	17.29 ± 5.43	26.98 ± 2.03	34.80 ± 11.61

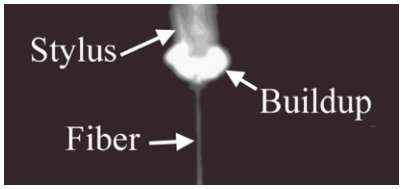

Figure 8. PMMA build-up on tungsten stylus accumulated during a single characterization trial.

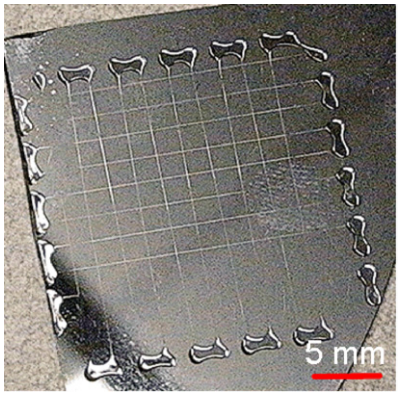

Figure 9. Weave pattern generated by the direct-write technique with 23% 495k g mol^{-1} PMMA solution.

capillary 500 μm again to make contact with the substrate, pausing for 1 s, and again raising the capillary 2 mm. In this manner, a wide variety of 'connect-the-dots' style geometries were produced including: a square wave, a weave pattern (figure 9) and a square 'spiral', in which several fibers drawn in series with increasing lengths, each oriented 90° relative to the previous fiber.

The primary advantage of the direct-write method is the elimination of the manual deposition of the pools at the terminal ends of each fiber (see figure 4). Eliminating this low-precision step increased the accuracy of fiber terminal placement as well as expedited the entire fiber fabrication process through further automation. The direct-write method also eliminated the uncontrollable stylus build-up seen in figure 8, which was suspected of contributing to the undesired variance in fiber diameter. Indeed, the fiber diameter standard deviation for the 23% PMMA 495k g mol^{-1} solution was only 2.70 μm, a value comparable to the lowest standard deviation achieved in table 1 with the Parylene® stylus. The average fiber diameter in this case was 10.25 μm, a value significantly lower than the corresponding average diameter (26.98 μm) produced using the Parylene®-stylus, suggesting that the drawing method itself influences the fiber diameter.

Table 2. Fiber yield: fraction of fabrication attempts that resulted in a complete, unbroken fiber for 495k g mol^{-1} PMMA solutions

Concentration (wt%)	Tungsten (%)	Glass (%)	Parylene (%)	Nonstick (%)
15.5	20	26	0	47
16	31	44	50	30
17	36	20	30	25
18	92	35	64	35
21.6	79	83	40	93
23	79	71	40	64

Table 3. Fiber yield: fraction of fabrication attempts that resulted in a complete, unbroken fiber for 950k g mol^{-1} PMMA solutions

Concentration (wt.%)	Tungsten (%)
13	36
15	93
18	78
21.3	71

3.3. Yield and uniformity of diameter in length

Fiber yield is defined as the number of unbroken fibers produced in a trial divided by the number of drawing passes attempted with the stylus during that trial. The yield values for the 495k g mol^{-1} and 950k g mol^{-1} trials are given in tables 2 and 3, respectively. Table 2 illustrates that fiber yield seems relatively independent of the stylus material. It should be noted that additional polymer concentrations ranging from 1% to 30% were tested, but it was found that only concentrations within the range listed in tables 2 and 3 produced nonzero yields. For the 495k g mol^{-1} solutions, the maximum yields (92% and 93%) were produced at an 18% concentration with the tungsten stylus and 21.6% concentration with the nonstick stylus, respectively. Additionally, a maximum yield of 93% occurred at the 15% concentration for the 950k g mol^{-1} solutions using a tungsten stylus. At PMMA concentrations below these optimum levels, smaller diameter fibers are formed, which leads to a higher fiber aspect ratio, defined as the ratio of length to diameter, and increased fiber fragility. This implies that fibers made from concentrations on the low end of the experimental spectrum and drawn to the required length of 1.8 mm will be very fragile. Thus, in order to increase the fiber yield, the concentration of the solution should be increased or the fiber length should be shortened. Yield also declined at high PMMA concentrations, with fibers generally fracturing rather than undergoing the surface tension-driven capillary break-up observed at low

Table 4. Coefficient of variation in diameter along the length of an individual fiber for 495k g mol^{-1} PMMA solutions.

Concentration (wt%)	Tungsten (%)	Glass (%)	Parylene (%)	Nonstick (%)
15.5	40	72	No data	11
16	29	22	26	12
17	27	40	16	16
18	15	22	14	20
21.6	19	9	7	8
23	18	7	20	12

Table 5. Coefficient of variation in diameter along the length of an individual fiber for 950k g mol^{-1} solutions.

Concentration (wt%)	Tungsten (%)
13	29
15	13
18	23
21.3	18

concentrations. This suggests that fibers produced from high concentrations are solidifying during the drawing process and fracturing under the tensile stress applied by the stylus during the draw.

No broken fibers were observed in any of the geometries fabricated with the direct-write method (with the 23% solution), illustrating the major advantage of the direct-write method over the Parylene® coated stylus (40% yield). However, comparison between the yield values should be carefully made due to fundamental differences between experimental parameters including: (1) geometric differences between the capillary and stylus; (2) varying fiber lengths drawn; and (3) differing substrate geometries. These experimental variances inevitably lead to differing diameters and fragilities, which directly impacts the fiber yield.

Measurements were taken along the length of each fiber to investigate diameter uniformity. SEM measurements were taken halfway along the length of the fiber and 50 μm from each terminal end of the fiber in order to avoid the initial necking/taper region that occurs at the interface between the fiber and the pool. Tables 4 and 5 show the coefficient of variation in diameter, which is defined as a ratio of the standard deviation of the diameter for a single fiber divided by the mean diameter of that specific fiber expressed in terms of a per cent value, calculated from these three measurements for the 495k g mol^{-1} and 950k g mol^{-1} solutions, respectively. Inspection of these tables indicates that the diameter of an individual fiber is less uniform when using solutions with low solid concentrations.

3.4. Fiber correlation to polymer solution properties

A comparison of the polymer solution's initial shear viscosity with the resulting fiber's diameter yielded a logarithmically increasing relationship between viscosity and fiber diameter for both molecular weights. The macroscopic explanation for this trend is as follows: when the fluid filament is drawn between the two pools of solution, it has a tendency to undergo surface tension-driven necking. If this is allowed to continue

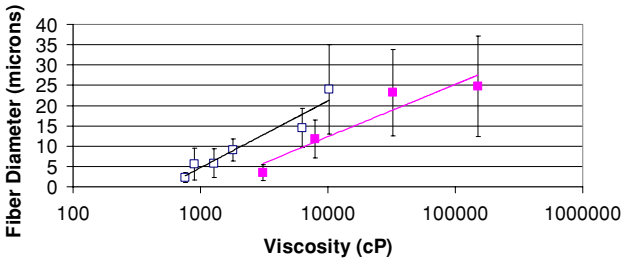

Figure 10. Fiber diameter as a function of viscosity. The data and fit are for the 950k g mol^{-1} solution (upper curve) and the 495k g mol^{-1} (lower curve) solutions.

for an extended period of time, the fiber diameter near the center of the filament will reach such a miniscule value that the fiber will fracture. Alternatively, if this necking is sufficiently impeded by a high solution viscosity, the filament solvent will evaporate before break-up, leaving a solid PMMA fiber. Additionally, because the viscosity influences the degree of surface tension-driven thinning before solidification, the steady-state fiber diameter can be controlled by the modulating viscosity. In this investigation, viscosity was controlled primarily by varying either the polymer concentration or the molecular weight. Increasing either (or both) of these two variables led to increased contact and entanglement between the randomly coiled PMMA molecules, resulting in a rapid rise in viscosity (figure 2) and, subsequently, fiber diameter (figure 10).

Tripathi *et al* [22] reported a correlation between a processability parameter P, and the creation of fibers drawn from a polymer solution (equation (1)). It was theorized that the fiber diameter increased with P, but this theory was only tested qualitatively. This phenomenon is quantitatively illustrated by plotting the fiber diameter versus P for each molecular weight in figure 11. Fiber diameter does indeed increase with increasing P ($D = 6.837\,\mathrm{Ln}(P) + 87.63$ with $R^2 = 0.9326$ for 495k g mol^{-1} solutions and $D = 5.2463\,\mathrm{Ln}(P) + 65.54$ with $R^2 = 0.8941$ for 950k g mol^{-1} solutions). Tripathi *et al* also reported that polymer solutions with P greater than 3×10^{-4} were drawn into unbroken fibers. Examination of figure 10 illustrates that relatively large fibers (>20 μm) will indeed form in this processability regime. However, smaller diameter fibers were drawn for polymer solutions with P as low as 4×10^{-6}. This discrepancy may be due to experimental differences between the two investigations. Specifically, the polymer solution filaments drawn in this experiment were formed relatively slowly (in ~10 s, compared to ~0.1 s in Tripathi's study). This allows filament drying to occur in partially drawn fibers, resulting in rapidly increasing viscosity (and therefore P) in some localities before the fiber is completely drawn. Another source of discrepancy may be due to the longer fibers drawn in [22], approximately 7 mm, resulting in same-diameter fibers that are inherently more fragile than those drawn to a length of ~2 mm, as in this study. Additionally, the processability parameter model assumes a Newtonian fluid, where in reality, a slight (~10%) degree of shear thinning, i.e. non-Newtonian fluid behavior, was observed for the 495k g mol^{-1} solution and 950k g mol^{-1} solution for shear rates ranging from 3.75 s^{-1} to 18.8 s^{-1} and 0.525 s^{-1} to 2.25 s^{-1}, respectively.

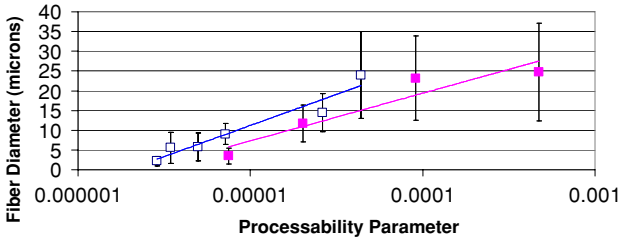

Figure 11. Fiber diameter as a function of the processability parameter. The data and fit are for the 950k g mol^{-1} solution (upper curve) and the 495k g mol^{-1} (lower curve) solutions.

The fact that the two curves in figure 11 do not overlap suggests that the process may be dependent on one or more additional variables. Ideally, if all undesired variables (such as solution buildup) could be eliminated, one parameter would exist that relates the intrinsic properties of a polymer solution to the expected fiber diameter. Figure 11 would have only one diameter value corresponding to each value of P, thereby accommodating rapid characterization of additional solvent/polymer/molecular weight sets since only the fluid (polymer solution) properties would need to be characterized to calculate P. However, the results presented in this paper show that P does not demonstrate independence of the process from molecular weight; therefore, additional parameters must still be considered.

4. Conclusion

Polymer micro- and sub-microscale fibers can be drawn from a polymer solution using a stylus controlled by a custom-made ultra-high-precision micromill. PMMA fibers ranging from sub-micron diameters to over 40 microns have been successfully fabricated over a 1.8 mm trench in a silicon substrate. Characterization of the micromill process indicated that the fiber diameter increased as the solid concentration in the polymer solution increased. It was also shown that increasing the molecular weight of the PMMA resulted in larger fiber diameters. Although other variables may influence fiber diameter (including temperature, drawing speed, stylus/capillary geometry, solvent volatility, open versus closed atmosphere, etc), the modulation of concentration and molecular weight provides a mechanism for controlling the fiber diameter. Additionally, the fiber diameter was observed to increase with an increase in the processability parameter, defined as a function of solvent evaporation rate, viscosity and surface tension.

A large variance between fibers drawn under the same experimental conditions was noted. A suspected culprit of this variance was the solidification of the solution on the stylus which accumulated during the drawing process. Several different stylus materials were tested in hopes of reducing this variance, and it was discovered that the stylus material did influence the severity of this variance with a Parylene®-coated stylus being influenced the least by accumulation. In addition, individual fiber diameter uniformity as low as 7% was achieved through control of these process parameters. It was also demonstrated that the stylus could be entirely replaced with a pressurized glass capillary filled with polymer solution. This micromill-controlled capillary was used to direct write complex fiber configurations with a low fiber diameter variance and high yield.

Acknowledgments

The authors would like to acknowledge Scott Cambron, Alex Isham and Mark Crain for instruction and fabrication assistance in this investigation. This work was supported by NSF grant ECS0506941, NASA Cooperative Agreement NCC5–571, NSF EPSCoR grant 6016955, DOE EPSCoR grant 46411101095 and the Commonwealth of Kentucky.

References

[1] Harfenist S A, Cambron S D, Nelson E W, Berry S M, Isham A W, Crain M M, Walsh K M, Keynton R S and Cohn R W 2004 Direct drawing of suspended filamentary micro- and nanostructures from liquid polymers *Nano Lett.* **4** 1931–7

[2] Tong L, Gattass R R, Ashcom J B, He S, Lou J, Shen M, Maxwell I and Mazur E 2003 Subwavelength-diameter silica wires for low-loss optical wave guiding *Nature* **426** 816–9

[3] Sperling L H 2001 *Introduction to Physical Polymer Science* 3rd edn (New York: Wiley-Interscience)

[4] Qin J, Gu J and Chung T 2001 Effect of wet and dry-jet wet spinning on the shear-induced orientation during the formation of ultrafiltration hollow fiber membranes *J. Membr. Sci.* **182** 57–75

[5] Mok S, Worsfold D J, Fouda A E, Matsuura T, Wang S and Chan K 1995 Study on the effect of spinning conditions and surface treatment on the geometry and performance of polymeric hollow-fiber membranes *J. Membr. Sci.* **100** 183–92

[6] Wienk I M, Olde Scholtenhuis F H A, van den Boomgaard T and Smolders C A 1995 Spinning of hollow fiber ulrtafiltration membranes from a polymer blend *J. Membr. Sci.* **106** 233–43

[7] Pereira C, Nobrega R, Peinemann K-V and Borges C 2003 Hollow fiber membranes obtained by simultaneous spinning of two polymer solutions: a morphological study *J. Membr. Sci.* **226** 35–50

[8] Yang S, Teo W K and Li K 2001 Formation of annular hollow fibers for immobilization of yeast passages *J. Membr. Sci.* **184** 107–15

[9] Zeng J, Saltysiak B, Johnson W S, Schiraldi D A and Kumar S 2004 Processing and properties of poly(methyl methacrylate)/carbon nano fiber composites *Composites* B **35** 173–8

[10] Wu G, Li Q and Cuculo J A 2001 Fiber structure and properties of poly(ethylene-2,6-napthalate) obtained by high speed melt spinning *Polymer* **41** 8139–50

[11] Wu G, Li H, Wu Y and Cuculo J A 2002 Structure and property studies of poly(trimethylene terephthalate high-speed melt spun fibers *Polymer* **43** 4915–22

[12] Samon J, Schultz J M and Hsiao B S 2002 Structure development in the early stages of crystallization during melt spinning *Polymer* **43** 1873–5

[13] Zachmann H G 1995 New insights into the structure and phase transitions of polymers *Nuclear Instrum. Methods Phys. Res.* B **97** 209–15

[14] Sandler J K, Pegel S, Cadek M, Gojny F, van Es M, Lohmar J, Blau W J, Schulte K, Windle A H and Shaffer M S P 2004 A comparative study of melt spun polyamide-12 fibers reinforced with carbon nanotubes and nanofibers *Polymer* **45** 2001–15

[15] Theron S A, Zussman E and Yarin A L 2004 Experimental investigation of the governing parameters in the electrospinning or polymer solutions *Polymer* **45** 2017–30

[16] Koski A, Yim K and Shivkumar S 2004 Effect of molecular weight on fibrous pva produced by electrospinning *Mater. Lett*. **58** 493–7
[17] Fong H, Chun I and Reneker D H 1999 Beaded nanofibers formed during electrospinning *Polymer* **40** 4585–92
[18] Deitzel J M, Kleinmeyer J, Harris D and Beck Tan N C 2001 The Effect of processing variables on the morphology of electrospun nanofibers and textiles *Polymer* **42** 261–72
[19] Doshi J and Reneker D 1995 Electrospinning process and applications of electrospun fibers *J. Electrostat*. **35** 151–60
[20] Kameoka J, Orth R, Yang Y, Czaplewski D, Mathers R, Coates G W and Craighead H G A 2003 Scanning tip electrospinning source for deposition of oriented nanofibers *Nanotechnology* **14** 1124–9
[21] Nain A S, Amon C and Sitti M 2004 Three-dimensional nanoscale manipulation and manufacturing using proximal probes: controlled pulling of polymer micro/nanofibers. *Proc. IEEE Int. Conf. Mechatronics* **3–5** 224–30
[22] Tripathi A, Whittingstall P and McKinley G H 2000 Using filament stretching rheometry to predict strand formation and 'processability' in adhesives and other non-Newtonian fluids *Rheol. Acta* **39** 321–37
[23] Byron Bird R, Armstrong R C and Hassager O 1977 *Dynamics of Polymeric Liquids: Fluid Mechanics* (New York: Wiley)
[24] White F M 1999 *Fluid Mechanics* (New York: McGraw-Hill)
[25] Friedrich C and Vasile M 1996 Development of the micromilling process for high aspect ratio microstructures *J. Microelectromech. Syst*. **5** 33–8